Journal of Molecular Structure 1006 (2011) 527–535

Contents lists available at SciVerse ScienceDirect

Journal of Molecular Structure

journal homepage: www.elsevier.com/locate/molstruc

Metallo-hydrazone complexes immobilized in zeolite Y: Synthesis, identification and acid violet-1 degradation

Ayman H. Ahmed *, M.S. Thabet

Department of Chemistry, Faculty of Science, Al-Azhar University, Nasr City, Cairo, Egypt

ARTICLE INFO

Article history:
Received 15 May 2011
Received in revised form 27 September 2011
Accepted 30 September 2011
Available online 8 October 2011

Keywords:
Zeolites
Hydrazone complexes
Diffusion method
Catalytic activity

ABSTRACT

Copper(II), cobalt(II) and nickel(II) complexes of hydrazone ligand (SAPH) derived from salicylaldehyde and phenylhydrazine have been encapsulated in zeolite-Y super cages via ship-in-a-bottle synthesis. Detailed characterization of the intrazeolitic complexes were performed by elemental analysis, spectral (FT-IR, UV–Vis.) studies, magnetic measurements and X-ray diffraction. Furthers, surface texture and thermal analysis (TG, DTG, DTA) have provided further evidence for successful immobilization of the metal complexes inside zeolite Y. Investigation of the stereochemistry of these incorporated chelates pointed out that, SAPH ligand is capable to coordinate with the central metal through the (C=N), phenolic (OH) and (NH) groups forming polynuclear structures. The involvement of zeolite oxygen in coordination was postulated in the hybrid materials. The intrazeolitic copper, cobalt and nickel–SAPH complexes have distorted tetrahedral, octahedral and square-pyramidal configurations, respectively. The zeolite encapsulated complexes are thermally stable up to 800 °C except Cu(II) sample which is thermally stable up to midpoint 428 °C. The assessment of the catalytic activity was performed by the use of the photo-degradation of acid violet-1 dye as a probe reaction in presence of H_2O_2 as an oxidant. Decolorization of acid violet-1 dye was examined under the same conditions whereas the unpromoted zeolite and Cu^{II}, Co^{II}, Ni^{II}–hydrazone complexes supported on zeolite showed 13% and 76%, 53%, 43% color removal, respectively. The results revealed that, the zeolite encapsulated Cu(II) complex generally exhibited better catalytic efficiency (76%) compared with other investigated zeolite encapsulated metal–hydrazone samples.

1. Introduction

Zeolites are a class of crystalline aluminusilicates based on rigid anionic frameworks with well-defined channels and cavities. The cavities contain exchangeable metal cations e.g., Na^+, K^+, Ca^{2+}, etc. The synthetic faujasite (FAU) type zeolite (Y or X) has the most widely studies on its utilizing as host materials. The FAU has a 12-ring window of diameter 0.74 nm and internal cavity about 11.2 nm. Actually, entrapment of metal complexes into zeolite leads to growing up the number of heterogeneous catalysts which combine the advantages of homogeneous and heterogeneous catalytic system, reduce the self-oxidation tendency of the complexes and promote the catalytic activity by dispersion of the complexes inside the zeolite pores. Heterogenization of metal complexes known to be active in homogeneous catalysis can be achieved by (i) polymerization of metal complex catalyst itself [1,2], (ii) immobilization of the metal complex on insoluble support e.g., polymers [3], and (iii) encapsulating it in the nanocavity of e.g., zeolites [4–9]. Fortunately, a wide variety of metal complexes have been successfully immobilized in a range of different zeolites where such hybrid materials have numerous applications including catalysis, gas separation, artificial photosynthesis and photocatalysis [4–11]. Schiff bases contain the azomethine group (—RC=N), including the employed hydrazone, can play a central role in development of heterogeneous catalysis owing to the great synthetic flexibility and they readily form stable complexes with most of the transition metals taking into account their catalytic and biological importance [12]. Thus, a substantial number of articles on the preparation and characterization of M–Schiff base complexes in the zeolite have been published [6–9,13]. A literature survey revealed that salicylaldehyde phenylhydrazone (SAPH) has antioxidant activity and can be used as an indicator for the titration of organometallic species [14]. Nevertheless, some chelates of SAPH [$M(SAPH)_2$, M = Cu(II) and Ni(II)] were synthesized under traditional conditions and characterized on the basis of elemental analysis with confirming spectroscopically [15], no work on their encapsulation in zeolite has been investigated besides the encapsulation process led to construction of different compositions and structures.

Currently, to meet the demand of green chemistry, it is favorable to use H_2O_2 as oxidant and H_2O as solvent for the oxidation reactions because H_2O_2 does not produce any side-product besides water. The role of transition metal complexes is overviewed for the

* Corresponding author.
E-mail address: ayman_haf5@yahoo.com (A.H. Ahmed).

0022-2860/$ - see front matter © 2011 Elsevier B.V. All rights reserved.
doi:10.1016/j.molstruc.2011.09.061

iron, copper and chromium compounds, for which photoreactivity is of crucial environmental importance. Attention is paid to these complex systems, in which metal centers are photoreduced by organic matter under solar irradiation and re-oxidized by molecular oxygen, i.e. to the systems, that play a part in the environmental photocatalysis. The photoreduction is accompanied by simultaneous oxidation of organic matter, which plays a role of ligand and/or sacrificial electron donor. Under favorable conditions a complete photodegradation of the organic pollutants can be achieved. The systems are more sophisticated due to concurrent generation of active oxygen species, such as the $O_2^{\cdot-}$, $HO_2^{\cdot}$, $OH^{\cdot}$, H_2O_2, and HO_2^-, which are involved in the redox reactions of the photocatalytic cycling and influence the pollutant degradation.

In this investigation, we described the synthesis and characterization of Y-zeolite encapsulated salicylaldehyde phenylhydrazone (SAPH) metal complexes [M = Co(II), Ni(II) and Cu(II)]. The structure of the ligand chosen for the studies is depicted in Fig. 1. The compositions and structures of the new zeolites, which are regarded as heterogeneous catalysts, were identified and tested for photodecomposition of acid violet-1 dye. The texture of the zeolites containing M(II)–SAPH complexes was described showing the possibility of using them as heterogeneous catalysts in other applications and in the same time to provide a conclusive evidence for the successful occlusion of the metallocomplexes within the zeolite matrix. The study is devoted on the zeolite encapsulated SAPH complexes as they represent new materials did not study before in contrast to employed M^{II}–Y.

2. Experimental

2.1. Materials and physical measurements

All the chemicals and solvents employed were of BDH or AR quality and used without further purification. The chemicals include Cu(II), Co(II) and Ni(II) acetates, salicyalaldehyde and phenylhydrazine. NaY zeolite (Lot No. D1-9915, HSZ-320N-NAA, Si/Al = 5.6) was obtained from Toyota Company Ltd., Japan, and used as received. The elemental analysis for carbon and nitrogen was estimated on Perkin Elmer 2400 at Microanalytical Unit of Cairo University, Egypt. The metal contents (w/w%) were determined by complexometric titration of EDTA using xylenol orange indicator, hexamine buffer and sodium fluoride as a masking agent for the interfering aluminum ions result from disintegration of the zeolite framework [16]. IR spectra were recorded as KBr pellet in the range 200–4000 cm^{-1} on a Mattson 5000 FT-IR spectrometer. Mass spectrum of the ligand was recorded on Shimadzu-GC.MS-QP 1000 EX using the direct inlet system at Cairo University, Egypt. UV–Vis. spectra of the samples in Nujol mull were measured in the range 200–1100 nm using a Perkin–Elmer lambda 35 UV–Vis. Spectrophotometer. The mass susceptibility of the solid materials (χ) was measured with a magnetic susceptibility balance of models Johnson Metthey and Sherwood. X-ray diffractograms were recorded using a Philips PW1840 X-ray powder diffractometer with Cu Kα target (λ = 1.54 Å). Thermal analyses (TG, DTG, and DTA) under flowing of dry nitrogen were carried out with a DTG-60 H thermal analyzer at Cairo University, Egypt. The surface texture characteristics obtained from nitrogen adsorption isotherms were determined at −196 °C using a conventional volumetric apparatus.

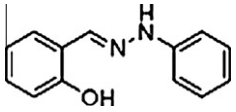

Fig. 1. Chemical structure of SAPH ligand.

BET-plots and *t*-curves estimated the specific surface areas (S_{BET}, S_t) where the samples were thermally degassed at 200 °C for 2 h prior to the adsorption measurements.

2.2. Preparations

2.2.1. Salicylaldehyde phenylhydrazone (SAPH)

The ligand is easily prepared in good yield from inexpensive starting materials and is simple to isolate in pure form. It was prepared according the method described in Ref. [14b]. Methanolic solution of phenylhydrazine (11 mL, 0.1 mol) and salicylaldehyde (10.5 mL, 0.1 mol) was refluxed for 2 h under constant stirring. The immediately formed yellow–white solid was collected by vacuum filtration, washed repeatedly by ethanol to remove any excess of reactants and finally dried in furnace at 80 °C for 3 h. The resulting ligand with the formula $C_{13}H_{12}N_2O$ was recrystallized from EtOH and melted at 142 °C (lit.mp 140–142 °C) [15,17]. The ligand structure was confirmed by IR spectroscopy and its purity was checked by mass spectrometry. The mass spectrum of the free ligand exhibited a molecular ion peak (M^+ value) at m/e = 212; calc. = 212.25. SAPH is air stable and easily soluble in most of organic solvents e.g., ethanol, chloroform, acetone and benzene.

2.2.2. Metal-exchanged zeolite (M^{II}–Y)

M^{II}–Y was generally prepared via the reversible ion exchange process [9b,c], which can be described by the following chemical equation.

$$Na^+-Zeolite(s) + M^{2+}(aq) \leftrightarrows M^{2+}-Zeolite(s) + 2Na^+(aq) \quad [M = Cu, Co \text{ and } Ni]$$

Seven grams of NaY was weighed out and treated at room temperature with 1500 mL 0.01 M acetate solution of M(II) ion [M = Cu, Co and Ni], the pH of the resulting heterogeneous mixture was in the 5–6 range. The mixture was conducted for 48 h with continuous stirring. After that, the powder was suction filtered off using a büchner and washed thoroughly by distilled water to remove the excess of adsorbed or unreacted ions till the washing solution was free from any M(II) ion content. The zeolite sample was then dried in air at room temperature for 24 h and finally stored over saturated ammonium chloride solution to maintain a constant humidity until required for use. The exchange level and metal content for the obtained solids are shown in Table 1.

2.2.3. Zeolite encapsulated metal complexes (Cu^{II}, Co^{II} and Ni^{II}(SAPH)/Y)

The intrazeolitic metallocomplexes were prepared using a solid–solid interaction technique by diffusing the ligand through the pores of preactivated M^{II}–Y to form a large and rigid complex becomes unable to escape from the zeolite cage (FL method). For this purpose, an amount of M^{II}–Y (2.0 g) was first activated by heating in a Pyrex shrink tube to 200 °C for 2 h in a vacuum of 10^{-4} Torr and then cooled to room temperature. Approximately 1.0 g of activated M^{II}–Y was intimately mixed with an excess of SAPH ligand (2.0 g) in a glove bag under nitrogen atmosphere. The finely powdered mixture was placed horizontally in a Pyrex shrink tube, evacuated again to 10^{-4} Torr for 10 min. and heated with constant stirring at 135 °C for 4 h. After the reaction was completed whereby the ligand diffuses freely through the channels and coordinates with metal ions, the furnace tube was cooled to room temperature, carefully opened and the products were washed in a beaker with successive portions of hot solvents (ethanol, acetone and methylene chloride, respectively). The product sample was then Soxhlet-extracted with acetone for 48 h at normal conditions to remove excess ligand that remained in the cavities of zeolite as well as located on the surface of zeolite along with neat complexes

Table 1
Physical and analytical data of SAPH and the zeolites used under investigation.

Sample label	Color	M.p*/Dec. temp. (°C)	*M* (wt.%)	Exchange level (%)	M/C, M/N found/calcd.	χ_g(c.g.s.)	Product assignment
SAPH	White	142*	–	–	–	–	–
NaY	White	>300	–	–	–	Diamag.	Y
Cu^{II}–Y	Pale blue	>300	6.8	77	–	1.14×10^{-5}	$[Cu(H_2O)_6]^{2+}$–Y
Co^{II}–Y	Pale pink	>300	5.0	57	–	1.04×10^{-5}	$[Co(H_2O)_6]^{2+}$–Y
Ni^{II}–Y	Pale green	>300	5.9	68	–	0.44×10^{-5}	$[Ni(H_2O)_6]^{2+}$–Y
Cu^{II}(SAPH)/Y	Dark green	>300	8.4	–	0.16/0.15, 1.04/1.0	0.004×10^{-5}	$[Cu_2(SAPH)(H_2O/O_z)_4]$–Y
Co^{II}(SAPH)/Y	Pale brown	>300	6.2	–	0.26/0.23, 1.8/1.5	1.02×10^{-5}	$[Co_3(SAPH)(H_2O/O_z)_{13}]$–Y
Ni^{II}(SAPH)/Y	Buff	>300	5.4	–	0.25/0.23, 1.7/1.5	0.42×10^{-5}	$[Ni_3(SAPH)(H_2O/O_z)_{11}]$–Y

* Melting without decomposition.

formed on the surface, if any. Finally, the solid was dried for 4 h at 100 °C in oven.

In comparison to the colors of M^{II}–Y and SAPH, new colors of M^{II}(SAPH)/Y composites have been acquired (Table 1). This observation beside the final preparation showed a nonextractable color related to SAPH complex by vigorous washing can be regarded as a direct evidence of encapsulation of SAPH complexes inside the zeolite pores.

2.3. Photocatalytic activity measurement

Photodecomposition experiments of acid violet-1 dye at λ_{max} 550 nm, (100 mL, 100 ppm) were carried out using UV Lamp (254 nm) of intensity 6 W. The suspension (catalyst + dye) that was stirred vigorously was left to equilibrate for 40 min in dark prior to illumination with UV Lamp, to ensure attaining complete adsorption and to monitor the change in dye concentration due to adsorption. Exposing the suspension to UV irradiation was then attained to stand on the photocatalytic activities of the catalysts. The UV–Vis. spectrophotometer JASCO V-570 unit, serial No. 29635 at scanning speed 4000 nm/mm was used for the determination of color intensity in the range of 190–700 nm. The calibration based on Beer–Lambert law was linear and used to quantify the dye concentration. Control experiments were carried out using UV irradiation without catalyst to check whether a direct photolysis for the dye occurred or not. In fact, the obtained activity of this experiment showed a very little effect on the dye degradation.

3. Results and discussion

Physical and analytical data of NaY, free SAPH, M^{II}–Y and M^{II}(SAPH)/Y (MCu^{II},Co^{II} and Ni^{II}) are listed in Table 1. The new hybrid materials are insoluble in common organic solvents. The slightly difference between the calculated and found (M/C, M/N) ratios in case of M^{II}(SAPH)/Y samples (Table 1) is plausibly due to insignificant unreacted part of M(II) ions in zeolite voids.

3.1. Spectral and magnetic studies

The IR spectra in the (4000–200 cm^{-1}) region provide information regarding the coordination mode in the modified zeolites and were analyzed by comparison with data of ligand (SAPH). The most relevant bands and proposed assignments for free ligand along with its corresponding M^{II}(SAPH)/Y (M = Cu, Co and Ni) as well as the host matrix are given in Table 2.

3.1.1. In comparison to NaY

It was noticed that the IR spectra of M^{II}–Y and M^{II}(SAPH)/Y are dominated by the Y zeolite bands assignable to surface hydroxyl groups, internal and external vibrations of tetrahedral geometry of the type (Si, Al)O_4 without any collapse in their crystallinity. As speculated, ion exchange of Na^+ ions by divalent cations would not change the infrared spectral feature of the hydrated zeolite since cation-framework interaction is usually weak in such case [18]. This fact in addition to the postulated large diameter of 12-ring window belong to faujasite-Y suggest the existence of the prepared M^{II}–Y samples (M = Cu, Co and Ni) in zeolite as aquo-complexes ($[M(H_2O)_6]^{2+}$) [9c]. Furthers, inspection of Table 2 showed that there is a somewhat distortion or dealumination in the zeolite lattice upon encapsulation of SAPH complexes owing to the changes in the positions, features and multiplicity of some structure-sensitive bands related to NaY [18]. This can be elucidated as follows: (1) The very weak pore opening band in NaY was varied to medium in Cu^{II}(SAPH)/Y, strong in Co^{II}(SAPH)/Y and weak with Ni^{II}(-SAPH)/Y. (2) The most significant shoulder band attributed to ν_{asym}T—O in NaY was shifted to lower frequency by 7 and 11 cm^{-1} for Cu^{II}(SAPH)/Y and Ni^{II}(SAPH)/Y respectively, in addition, it was splitted into two strong bands (1143 and 1099 cm^{-1}) in case of Co^{II}(SAPH)/Y. As the zeolite-Y containing the complex is still retaining its crystallinity as observed from the IR spectra and demonstrated by XRD later, the most probable to occur is the distortion. Perhaps the lower shift in the position of the structure sensitive bands results from the weak deformation in the framework. This deformation in the zeolite topology arise from generation of M—O(zeolite) linkage in M^{II}(SAPH)/Y samples.

3.1.2. In comparison to free SAPH ligand

The bands due to the encapsulated complexes are weaker due to a low concentration as seen from the metal contents (Table 1). Thereby, the encapsulated complexes can only be observed in the regions where the zeolite matrix does not absorb (1200–1600 cm^{-1}). Indeed, FT-IR data pointed out SAPH can coordinate to the metal ions via the azomithinic nitrogen (—C=N—), phenolic oxygen (C—O) and (NH) group. This was concluded based on: (1) the lower shift in the azomethine (C=N) group upon complexation substantiates the involvement of the azomethine in coordination. (2) The higher frequency shift of the band assigned to phenolic ν(C—O) stretching by chelation suggests the coordination through the phenolic oxygen. Note the large shift to the higher frequencies of the phenolic (C—O) is going from a hydrogen bonded structure to a covalent metal bonded structure. In addition to the above, the observation of $\nu(OH)_{phenolic}$ at nearly the same position in case of Cu^{II}(SAPH)/Y reflects the deprotonation of OH which is protonated in cases of Co^{II}(SAPH)/Y and Ni^{II}(SAPH)/Y owing to its disappearance. (3) The obscure of ν,δ(NH) in Co^{II}(SAPH)/Y indicates the deprotonation of this group while its shift towards lower side in Cu^{II}(SAPH)/Y and Ni^{II}(SAPH)/Y suggests its deprotonation. In the low frequency region of the spectra there are bands of moderate intensity, which can probably assigned to the M—O and M—N vibrations at nearly 400–450 and 500–550 cm^{-1}, respectively. Occasionally, some of these bands are merged with the Y bands (Table 2). The appearance of these bands supports the coordination mode of ligand and confirms its interaction with the exchanged metal ions. Bands appearing at 1496, 1418 (SAPH), 1457, 1435 (Cu^{II}(SAPH)/Y), 1492, 1478, 1457 (Co^{II}(SAPH)/Y), and 1491, 1465 (Ni^{II}(SAPH)/Y) cm^{-1} are the usual modes of phenyl ring vibrations.

Table 2
IR spectral data of SAPH, NaY and the encapsulated metallo-hydrazone complexes.

Sample	Internal vibrations			External vibrations				Adsorbed water	ν,δ (NH)	δ (OH) phenolic	ν(C=N)	ν(C—O) phenolic	δ(OH) in plane
	ν_{asym}T—O	ν_{sym}T—O	T—O_{bend}	D—R	Pore opening	ν_{sym}T—O	ν_{asym}T—O						
SAPH	–	–	–	–	–	–	–	–	3288, 1538	1360	1602	1272	–
NaY[a]	1032	720	463	576m	390vw	787m	1140sh	3456br, 1638	–	–	–	–	–
Cu^{II}(SAPH)/Y	1018	716	458	576m	381m	787m	1133sh	3460br, 1623	3247,1520[b]	1353	1540	1321	1400
Co^{II}(SAPH)/Y	1011	722	462	578m	354s	791m	1143s, 1099s	3460br, 1623	–	–	1556	1307	1400
Ni^{II}(SAPH)/Y	1023	713	460	583m	371w	789m	1129sh	3430br, 1635	3240[c], 1524	–	1556	1319	1400

[a] Reported in literature [9a,c].
[b] Emerged with ν(C=N).
[c] Dominated by zeolite bands.

The previously bands corresponding to phenyl ring reveal small shifts in the resulted complexes than free ligand, this is usual due to the expected symmetry and electronic structure changes upon complexation. Coordinated water in the host–guest materials, M^{II}(SAPH)/Y, was supposed based on the appearance of the bands attributed to δ(OH) in plane at 1400 cm^{-1} [19]. Other bands ascribed to coordinated water that would be expected to appear at 600–1100 and 1600–1680 cm^{-1} have not been noticed owing to their overlap with Y bands.

The UV–Vis. Spectra confirm the incorporation of metalloSAPH complexes into the zeolite NaY super cages. Fig. 2. shows the absorption spectra of ligand (SAPH) along with its related M^{II}(-SAPH)/Y. The main characteristic bands for SAPH ligand are observed at 399, 349, 324 and 245 nm, which are assigned to $n \rightarrow \pi^*$ (—C=N—), $\pi \rightarrow \pi^*$ (—C=N—), $\pi \rightarrow \pi^*$ (phenolic ring) and $\pi \rightarrow \pi^*$ (phenyl ring), respectively. Apart from L and NaY bands, the investigated M^{II}(SAPH)/Y exhibited new bands related to d–d transition showing the configuration around the metal ion of the encapsulated complex. Cu^{II}(SALSC)/Y showed two bands at 553 and 824 nm assigned to charge-transfer (L → M) and $^2B_2 \rightarrow {}^2E_2$ transition in a pseudo tetrahedral structure around the Cu(II) ions [20]. Co^{II}(SAPH)/Y sample exhibited two absorption bands at 544 and 741 nm which are probably assigned to $^2T_{1g} \rightarrow {}^4T_{1g}$(P) and $^2T_{1g} \rightarrow {}^4A_{2g}$ in an octahedral geometry around the Co(II) ions [21a,b]. Ni^{II}(SAPH)/Y sample revealed two bands at 719 and 515 nm attributed to $^3E(P) \rightarrow {}^3B_2(F)$ and $^3E(P) \rightarrow {}^3E(F)$ transitions, respectively. The observation of these bands suggests a prevailing square-pyramidal configuration around Ni(II) ion [21a].

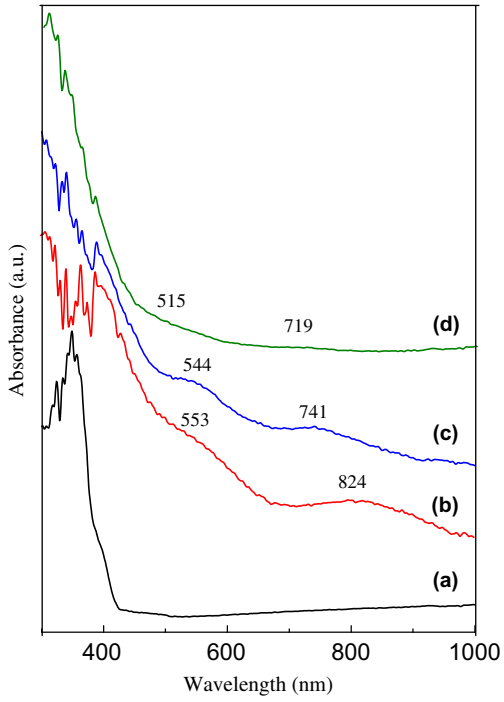

Fig. 2. Electronic spectra of (a) SAPH, (b) Cu^{II}(SAPH)/Y, (c) Co^{II}(SAPH)/Y and (d) Ni^{II}(SAPH)/Y.

Indeed, magnetic measurements for this type of materials give limited information because the molecular weights for these heterogonous samples are undetermined and the encapsulated complexes are not neutral by which we can ignore the diamagnetic effect of zeolite. We have encapsulated cationic complexes neutralized by the negative charges on the crystalline aluminuslicates (zeolite-Y) and connected in the same time with the zeolite oxygen as confirmed from the IR data. Thereby, it becomes impracticable to calculate the effective magnetic moments (μ_{eff}) that require the knowledge of the molecular weight assigned to the occluded complexes [9a,b,d,e]. The very low paramagnetic value of χ_g for Cu^{II}(SAPH)/Y (Table 1) indicates that the Cu(II) ions are so close to each other that leads to incomplete quenching of the spin moments of the ions. This means that the supposition of Cu—Cu bond in the molecular structure is not excluded specially the obtained χ_g value agrees to a great extent with this conclusion. But the proposed structure shown in Scheme 2 grants the formation of stable five membered chelate ring around the copper ion along with approaching of the two copper ions that quenches of the spin moments. The paramagnetic value of χ_g in case of Co^{II}(SAPH)/Y (Table 1) is consistent with high spin octahedral geometry around the Co (II) ion. This configuration is preferred than the low spin on the basis: (1) the ligand has strongly electronegative donor atoms (oxygen, nitrogen) and has little tendency to form π bonds with the metal ions, (2) if the low spin octahedral complex was formed, the high energy e_g orbitals must contain one electron $[(t_{2g})^6 (e_g)^1]$ and this makes the octahedral complex too unstable to exist. This fact allows $[Co^{II}(CN)_5]^{3-}$ is formed instead of an octahedral $[Co^{II}(CN)_6]^{4-}$ in case of π acceptor ligand as cyanide ion. Indeed, thermal analysis (DTA curve) studied later supports this point referring to the high thermal stability of Co^{II}(SAPH)/Y. Accordingly, the room temperature magnetic moment assigned to the high spin Co^{II}(SAPH)/Y $[(t_{2g})^5 (e_g)^2]$ is expected to be found near 3.9 B.M. (spin only moment) owing to the existence of three unpaired electrons. Also, the paramagnetic nature of square-pyramidal Ni^{II}(SAPH)/Y that indicated from the χ_g value (Table 1)

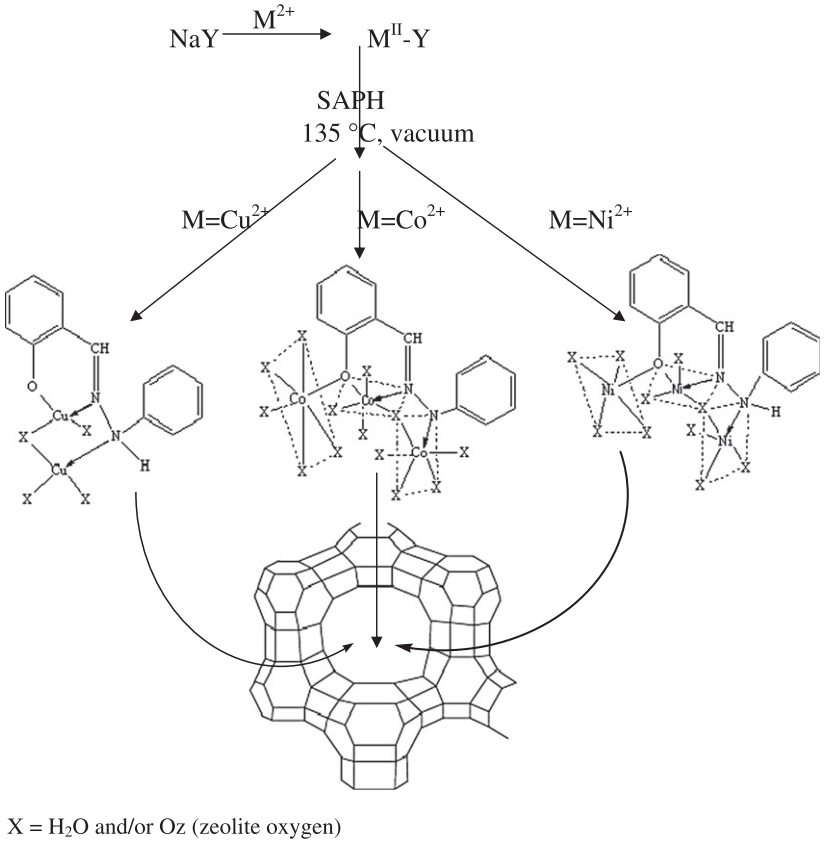

Scheme 1. Synthesis and postulated structures of zeolite encapsulated metallo-hydrazone complexes.

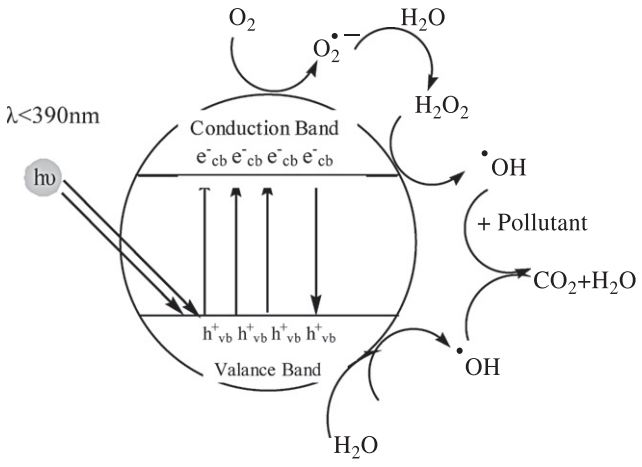

Scheme 2. Proposed mechanism of the photocatalysis.

suggests a high spin arrangement ($S = 1$). This C_{4v} symmetry is also proposed on the basis of the most favorable ligands for high spin 5-coordinate nickel complexes have strongly electronegative donor atoms (oxygen, nitrogen, halogens) and are weak π acceptor [21c]. Expected magnetic moment for Ni^{II}(SAPH)/Y sample is believed to be correct near 2.8 B.M. (spin only value). The comparable values of χ_g assigned to Co^{II}, Ni^{II}–Y with that of their corresponding complexes may be taken as an argument for the absence of M—M bond in such cases.

In the light of the forgoing results discussed above, the diffusion synthesis method showing the most likely structures of accommodated metalloSAPH chelates inside the zeolite matrix can be

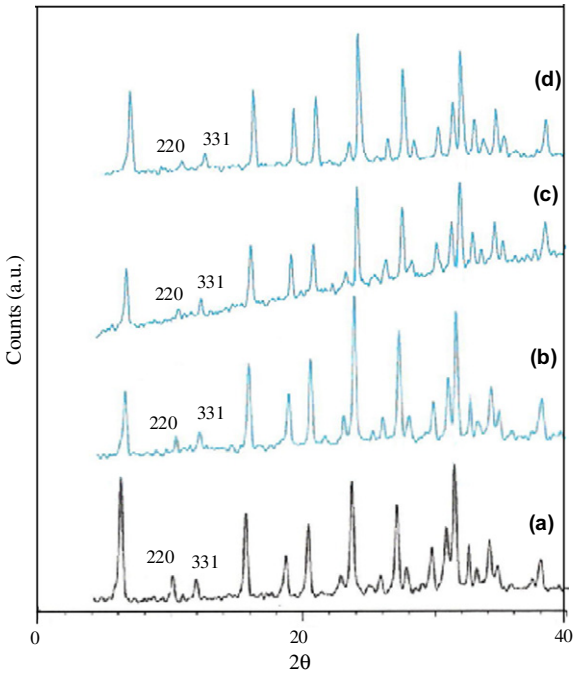

Fig. 3. X-ray diffraction patterns of (a) NaY, (b) Cu^{II}(SAPH)/Y, (c) Co^{II}(SAPH)/Y and (d) Ni^{II}(SAPH)/Y.

represented by Scheme 1. Negative zeolite oxygen and deprotonated ligand compensate the positive charges on the metal ions. At the first glance, the resulting structures may be unacceptable due to the presence of more than one metal ion. But in fact they

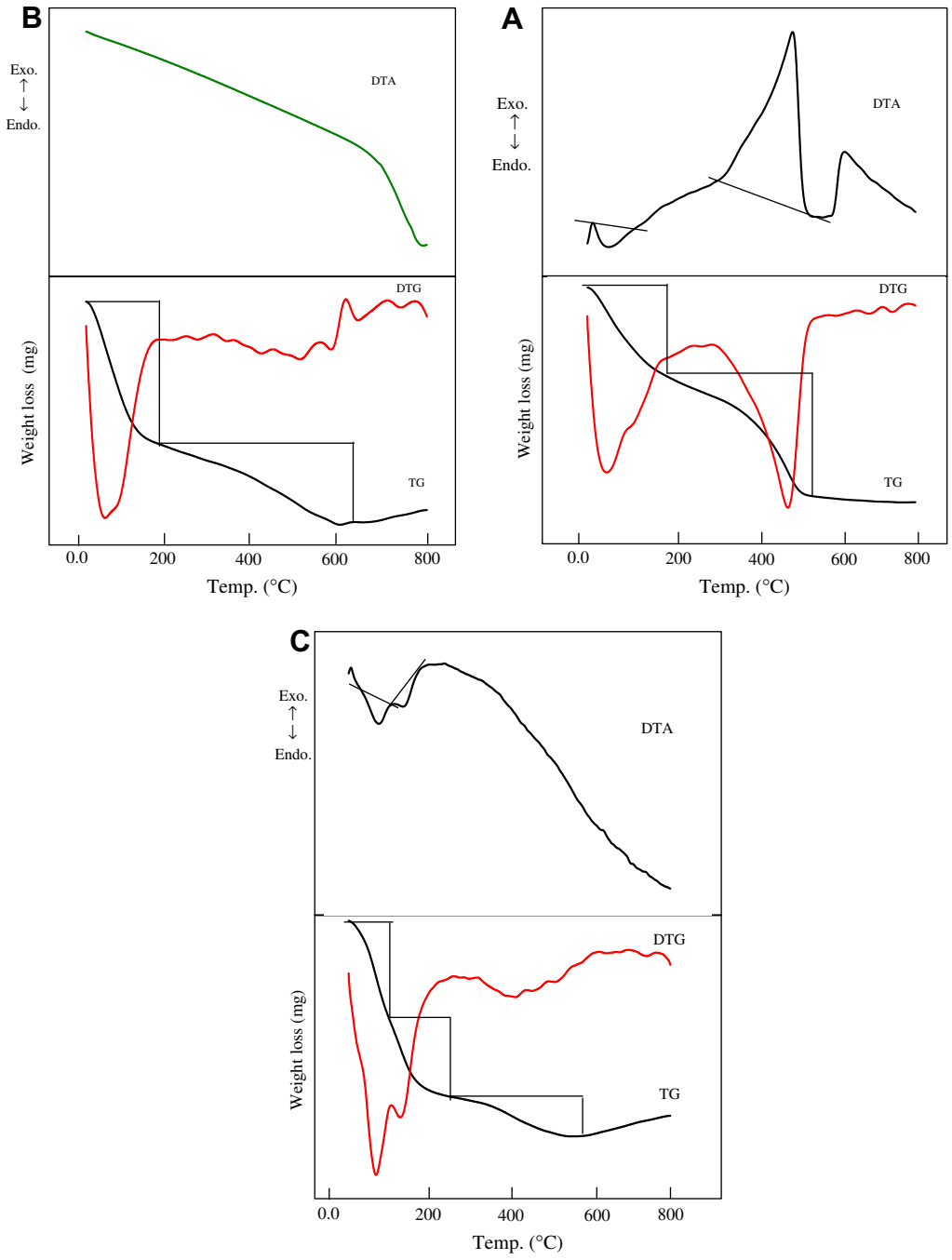

Fig. 4. TG, DTG and DTA curves of (A) Cu^{II}(SAPH)/Y, (B) Co^{II}(SAPH)/Y and (C) Ni^{II}(SAPH)/Y.

were presumed on the basis: (1) the elemental analysis was repeated, (2) an excess of ligand was added, (3) the washing process was performed vigorously (4) the ligand has versatile coordination sites and (5) the preparation circumstances are untraditional. In spit of the chemical structures are well authenticated by single crystal X-ray, we cannot isolate a single crystal from heterogonous materials. Otherwise, if we try to separate the encapsulated metal(II)SAPH complexes or prepare them in free state, we expect to obtain differ complexes since (1) the resulting data ascertained the involvement of zeolite oxygen in coordination, (2) the encapsulated metal(II)SAPH complexes are cationic complexes neutralized by negative charges on zeolite framework and not neutral complexes, (3) In many cases, the entrapment of the complex in the zeolite leads to construction of new composition and structure differs from the free one owing to the zeolite restriction, (4) the spatial constraints imposed by the dimensions of the zeolite cage leads to the distortion in the immobilized complex structure and allow approaching of ligand to the metal ions thus the probability of polynucleating bonding increases specially when number of metal ions presented in zeolite cavities are in excess compared with the ligand molecules considering the size of ligand molecule is larger.

3.2. XRD studies

Further arguments confirming the accommodation of M^{II}(SAPH) complexes (M = Cu, Co and Ni) inside the zeolite cages were provided by XRD technique. X-ray diffraction patterns (Fig. 3) of NaY

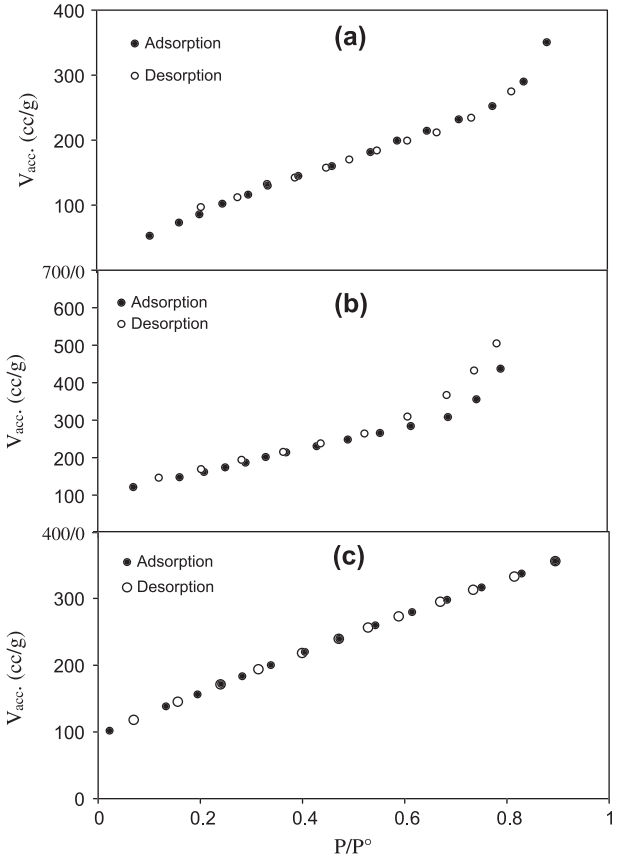

Fig. 5. N_2-adsorption–desorption isotherms of (a) Cu^{II}(SAPH)/Y, (b) Co^{II}(SAPH)/Y and (c) Ni^{II}(SAPH)/Y.

as well as the zeolite encapsulated metallocomplexes were recorded at 2θ values between 6° and 70°. The peaks observed in all patterns are essentially similar and no new peaks were detected. As the XRD is a surface analytical technique and there is a difference in colors of SAPH, NaY and M^{II}–Y by encapsulation (Table 1), the obscure of new peaks attributed to neat complexes provides an evidence to the residing of the metallocomplexes inside the zeolite cavity and not on the external zeolite surface. Interpretation of the obtained XRD data in accordance to the published NaY [9e] can be shown as follows. It was reported that the diffraction pattern for NaY could be fitted in terms of a cubic lattice with $I_{220} > I_{311}$ [9e,22]. Our data showed that the crystallinity of zeolite Y is almost preserved after entrapment of the SAPH complexes in it. The relative intensities of the 3 1 1, 2 2 0 reflections in published NaY ($I_{220} > I_{311}$) was varied upon inserting the complexes, i.e. $I_{311} > I_{220}$ in case of M^{II}(SAPH)/Y patterns. This can be explained on the basis the replacement of sodium cations in NaY by large complex molecules (M^{II}(SAPH)) leads to disturb the random distribution of small extra framework cations [23] and this change in the location of small cations influences the relative intensities of 3 1 1, 2 2 0 peaks. This of course indicates that the entrapped large metallocomplexes displaced the sodium ions from their random positions in the super cages to locations of sodalite and center of a single six-ring (S6R) [24] residing inside the large cavity of zeolite Y. Worthy mention, the changes in the charge distribution within the cavities and channels leads to alter the adsorption behavior as well as the catalytic activity.

3.3. TGA and DTA studies

In fact, execution the percentage decomposition of components of Cu(II), Co(II) and Ni(II) complexes and correlate it with total molecular weight of complexes would expect to be inaccurate and the calculations are not adequate. The reason for this arises from the fact that the molecular weights of the samples are undetermined as we deal with composite materials. We may have several numbers of encapsulated complex molecules dispersed in one supercage or one unite cell of zeolite. Nonetheless, thermal analysis can provide some information about the influence of zeolite shielding on the thermal stability of metalloSAPH complexes. Thermograms (TG, DTG and DTA) of the investigated hybrid materials (M^{II}(SAPH)/Y, M = Cu, Co and Ni) have been studied and shown in Fig. 4.

TG curve of Cu^{II}(SAPH)/Y showed two sets of bands in the 35–150 and 150–450 °C regions. DTA curve agreed with the above result and showed one endothermic peak at 75 °C and another exothermic peak at 428 °C. The former is due to water removal from the zeolite-Y voids while the latter reflects the complex decomposition because it is accompanied by weight loss as clear from the TG curve. For Co^{II}(SAPH)/Y, TG curve exhibited also two decomposition stages starting at 50 and 200 °C for the desorption of water from the interacrystalline voids of zeolite. DTA curve did not show any weight loss exothermic peak assignable to the decomposition of Co^{II}(SAPH) up to 800 °C referring to its high thermal stability. In the case of Ni^{II}(SAPH)/Y, TG curve showed three stages of decomposition starting at 30, 110 and 270 °C related to the removal of trapped and intra-zeolite water. The first two peaks are accompanied by endothermic effect while the third was not observed. No exothermic effect has been noticed by DTA measurement within the range 30–800 °C considering the high thermal stability of the occluded Ni(II) complex.

Thermal analysis conspicuously indicates that the formation of the complexes inside the zeolite cages increases their thermal stability up to a noticeable degree due to the zeolite shielding effect.

3.4. Surface studies

The texture of a catalyst surface, namely, the specific surface area and pore geometry are of prime importance in determining the activity, sometimes, also the selectivity of the solid catalyst [25]. From this point of view, surface texture of the synthesized samples is necessary to be considered.

Nitrogen isotherms of M^{II}(SAPH)/Y (M = Cu, Co and Ni), Fig. 5, have been carried out and compared with that of the published

Table 3
Some surface characteristic data of NaY and its corresponding zeolite encapsulated complexes.

Sample label	BET (m^2/g)	S_t (m^2/g)	V_p (cm^3/g)	$\bar{r}$ (Å)	V_{mic} (cm^3 g)	V_{mes} (cm^2/g)	S_{mic} (m^2/g)	S_{wide} (m^2/g)	S_{ext} (m^2/g)	Microporsaty %
NaY[a]	902	758	0.80	22.2	0.59	0.21	226	676	90	74
Cu^{II}(SAPH)/Y	502	455	0.56	27.7	0.30	0.26	268	234	212	54
Co^{II}(SAPH)/Y	606	606	0.68	28.1	0.66	0.02	588	18	201	97
Ni^{II}(SAPH)/Y	597	598	0.59	24.7	0.49	0.10	156	18	101	83

Note: (S_{BET}) BET-surface area; (S_t) surface area derived from V_{t-t} plots; (S_{mic}) surface area of micropores; (S_{mes}) surface area of mesopores; (S_{ext}) external surface area; (V_p) total pore volume; (V_{mic}) pore volume of micropores; (V_{mes}) pore volume of mesopores; ($\bar{r}$) mean pore radius.

[a] Reported in literature [9c].

NaY [9c] which is typical of microporous solid and type I of Brunauer classification [26]. Some surface parameters of NaY and its related encapsulated complexes have been collected in Table 3. The obtained data showed that Cu^{II}(SAPH)/Y, Co^{II}(SAPH)/Y and Ni^{II}(SAPH)/Y materials have a Brunauer classification of type II (without hystresis loop), type II (with hystresis loop) and a medium type between I and II (without hystresis loop), respectively. Perhaps, the absence of hystresis loop indicates the nonporous nature due to the filling of the zeolite pores by SAPH complexes, but their large computed surface areas (Table 3) ascertain they still have porous natures. In comparison to the published NaY isotherms, all the prepared M^{II}(SAPH)/Y solids exhibited a decrease in the N_2 adsorption capacity pointing to filling of the zeolite pores by metal complexes. On the other hand, the V_{l-t} construction of M^{II}(SAPH)/Y samples exhibited (i) a little upward deviation in cases of Cu^{II}(SAPH)/Y and Ni^{II}(SAPH)/Y acquiring a wide porosity while (ii) an upward and downward deviation for Co^{II}(SAPH)/Y indicating the existence of wide and narrow pores mixture. The specific surface areas (S_t) for these composite materials were determined from the V_{l-t} plots and are in close agreement with (S_{BET}) indicating the correct choice of the standard *t*-curves. As the zeolite framework structure did not collapse by encapsulation as shown from the IR and XRD patterns, the reduction of surface areas and total pore volumes of modified zeolites upon introducing the metallohydrazone complexes provides a direct evidence for the existence of the complexes inside the cavities and in the same time refers to the filling degree of the zeolite pores.

3.5. Photocatalytic activity

No disappearance of acid dye was observed without UV irradiation. A diverse disappearance of acid dye could only be observed with the simultaneous presence of different samples and of UV light, as shown in Fig. 6. This indicates that the system is working in a real photocatalytic regime. Co^{II}(SAPH)/Y sample showed a photocatalytic activity close to that has been exhibited by Ni^{II}(SAPH)/Y complex. This may be due to the immobilization on the interior and external surface of the support. Under the same conditions, the parent zeolite and Cu^{II}, Co^{II}, Ni^{II}(SAPH)/Y showed 13% and 76%, 53%, 43% color removal of acid dye, respectively. It is worth to mention that, degradation of azo-dye by some transition metal oxides supported on ZSM-5 zeolite characterized by a similar behavior [27]. Under UV, Fig. 7, acid violet dye gets excited and can cede an electron to the valence band of metal-centered orbital via an attack by ·OH radicals [28]. Under visible light, only acid violet dye becomes excited with the promotion of an electron in an upper orbital, whose relative energy level enables the transfer of one electron into the conduction band of the iron in the catalyst. The present photo-bleaching of acid violet dye only corresponds to decolorization by loss of conjugation of the double bonds in the whole molecule induced by the electron transfer to complex. The data obtained within the first 30 min, Fig. 8, were used for kinetic correlation according to pseudo first-order equation [$\ln(C/C_o) = k_a t$] [29,30], and the apparent first-order rate constants (k_a) are listed in Table 4. The catalytic activities follow the order of Cu^{II}(SAPH)/Y > Co^{II}(SAPH)/Y > Ni^{II}(SAPH)/Y > NaY. The Cu^{II}(SAPH)/Y sample has the highest acid dye decolorization capacity, whose k_a is 2.59×10^{-1} min^{-1}, which is higher than reactions catalyzed by Co^{II}(SAPH)/Y and Ni^{II}(SAPH)/Y. The main reaction mechanism for decolorization of dye can be described by Scheme 2 and elucidated by the following equations [29–32]:

$$\text{Dye} + h\nu \rightarrow \text{dye}^* \quad (1)$$

$$\text{M(II) site} + \text{dye} \rightarrow \text{M(I) sites } (e^-) + \cdot\text{dye}^+ \quad (2)$$

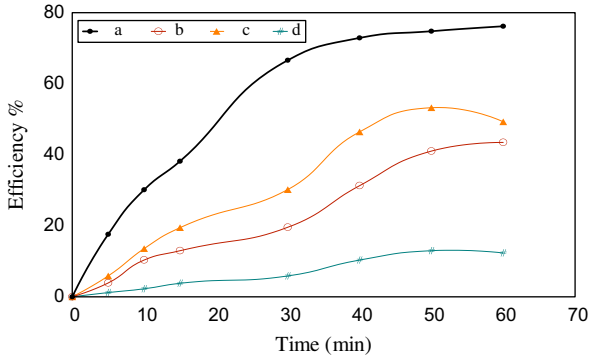

Fig. 6. Effect of time on the degradation of acid violet-1 dye in the presence of (a) Cu^{II}(SAPH)/Y, (b) Ni^{II}(SAPH)/Y, (c) Co^{II}(SAPH)/Y and (d) NaY zeolites.

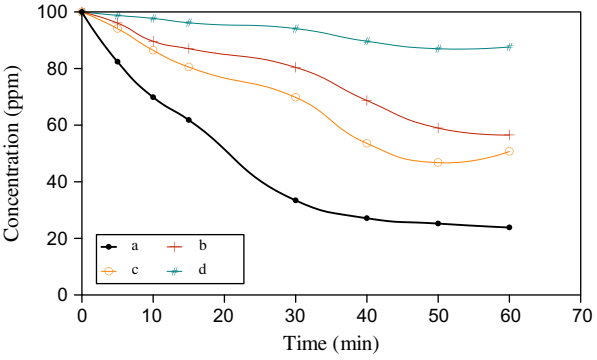

Fig. 7. Decolorization of acid violet-1 dye by (a) Cu^{II}(SAPH)/Y, (b) Ni^{II}(SAPH)/Y, (c) Co^{II}(SAPH)/Y and (d) NaY samples.

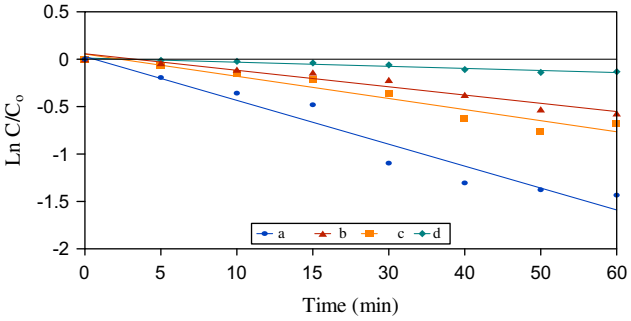

Fig. 8. Pseudo first-order plots of (a) Cu^{II}(SAPH)/Y, (b) Ni^{II}(SAPH)/Y, (c) Co^{II}(SAPH)/Y and (d) NaY for acid violet degradation at specific conditions.

Table 4
Kinetics rate of the dye removal using the catalytic oxidation.

Sample	K (min^{-1})	R^2 correlation coefficient
NaY	0.0341	0.9694
Cu^{II}(SAPH)/Y	0.2593	0.9708
Co^{II}(SAPH)/Y	0.1708	0.9652
Ni^{II}(SAPH)/Y	0.1441	0.9739

$$H_2O_2 + \text{Cu(II) sites } (e^-) \rightarrow \text{Cu(I) sites} + \text{Highly oxidative radicals} \quad (3)$$

$$\text{Highly oxidative radicals} + {}^{\cdot}\text{dye}^{+} \rightarrow CO_2 + H_2O + \text{Mineralization Product} \quad (4)$$

$$\text{Highly oxidative radicals} + \text{Cu(I) sites} \rightarrow \text{deactivated radicals} + \text{Cu(II) sites} \quad (5)$$

$${}^{\cdot}\text{dye}^{+} + \text{Cu(I) sites} \rightarrow \text{dye} + \text{Cu(II) sites} \quad (6)$$

Eqs. (1)–(4) describe the formation of highly oxidative radicals and the degradation processes of the dye, while Eqs. (5) and (6) describe the quenching of highly oxidative radicals and the deactivation of the free radical intermediate of the dye.

4. Conclusions

The results suggest that transition metal complexes of SAPH ligand [M = Cu(II), Co(II) and Ni(II)] can be accommodated in the super cages of zeolite-Y by FL method without any strain. Spectroscopic techniques, chemical analysis, magnetism, thermogravimetric and XRD patterns as well as surface area and nitrogen adsorption measurements prove to be essential tools for identifying and characterizing the metal(II) species formed inside the zeolite-Y. The results showed that, SAPH can coordinate to Cu(II), Co(II) and Ni(II) ions through the (C=N), phenolic (OH) and (NH) groups forming numerous structures around the central metal atom. The resulting compositions and structures for the encapsulated complexes are differ from those formed under ordinary conditions due to the zeolite constraints and the different synthesis conditions. The involvement of zeolite oxygen (Oz) in coordination was suggested assuming the change in the positions and features of some zeolite sensitive bands. The immobilized SAPH complexes have greater thermal stability due to the zeolite shielding. It is authenticated by catalytic activity results that, decolorization of dye is facilitated by presence of zeolite encapsulated Cu(II), Co(II) and Ni(II)–hydrazone complex catalysts, M^{II}(SAPH)/Y. Comparison of the photocatalytic activity of different catalysts has clearly showed that Cu^{II}(SAPH)/Y is better photocatalyst for decolorization of acid violtet-1 dye (76%). Photocatalytic decolorization reaction follows pseudo-first order kinetics.

References

[1] R. Ando, H. Ono, T. Yagyu, M. Maeda, Inorg. Chim. Acta 357 (2004) 817.
[2] M.R. Maurya, A. Kumar, J. Mol. Cat. A: Gen. 250 (2006) 190.
[3] D.C. Sherrington, Catal. Today 57 (2000) 87.
[4] K.J. Balkus Jr, A.G. Gabrielove, in: N. Herron, D. Corbin (Eds.), Inclusion Chemistry with Zeolites, Nanoscale Materials by Design, Kluwer, Dordrecht, 1995, p. 159.
[5] F. Bedioui, Coord. Chem. Rev. 144 (1995) 39.
[6] M.S. Niasari, M. Shaterian, J. Porous Mater. 15 (5) (2008) 581.
[7] J. Poltowicz, K. Pamin, E. Tabor, J. Haber, A. Adamski, Z. Sojka, Appl. Catal. A: Gen. 299 (2006) 235.
[8] M.R. Maurya, S.J.J. Titinchi, S. Chand, J. Mol. Catal. A: Gen. 214 (2004) 257.
[9] (a) A.H. Ahmed, J. Mol. Stuct. 839 (2007) 10;
(b) A.H. Ahmed, J. Appl. Sci. Res. 3 (12) (2007) 1663;
(c) T.M. Salama, A.H. Ahmed, Z.M. El-Bahy, Micropor. Mesopor. Mater. 89 (2006) 251;
(d) Ayman H. Ahmed, Zeinhom M. El-Bahy, Tarek M. Salama, J. Mol. Struct. 969 (2010) 9;
(e) A.H. Ahmed, A.G. Mostafa, Mater. Sci. Eng. C – Biol. Sci. 29 (2009) 877.
[10] G.A. Ozin, C. Gil, Chem. Rev. 89 (1989) 1749.
[11] P.A. Jacobs, Stud. Surf. Sci. Catal. 157 (2005) 289.
[12] (a) D.X. West, A.E. Libertia, S.B. Padhye, P.B. Chikate, A.S. Sonawane, Coord. Chem. Rev. 123 (1993) 49;
(b) Martinez, C. Hemmert, H. Gornitzka, B. Meunier, J. Organomet. Chem. 690 (2005) 2163;
(c) G. Cerchiaro, G.A. Micke, M.F.M. Tavares, A.M.C. Ferreira, J. Mol. Catal. A: Chem. 221 (2004) 29;
(d)J. Mol. Catal. A: Chem. 202 (2003) 253.
[13] M.R. Maurya, A.K. Chandrakar, S. Chand, J. Mol. Catal. A: Gen. 263 (2007) 227.
[14] (a) E.I. Pleskushkina, A.N. Nikolaevskii, T.A. Filippenko, Russ. J. Appl. Chem. 174 (5) (2001) 793;
(b) B.E. Love, E.G. Jones, J. Org. Chem. 64 (1999) 3755.
[15] (a) L. Hanter, I.A. Marriott, J. Chem. Soc. (1937) 2000;
(b) T.V. Troepol'skaya, E.N. Munin, Z.S. Titova, Yu.P. Kitaev, Russ. Chem. Bull. 27 (1978) 777.
[16] A.I. Vogel, A Text Book of Quantitative Inorganic Analysis, fourth ed., Longman, London, 1989.
[17] Z. Rappoport (Ed.), Handbook of Tables for Organic Compound Identification, third ed., The Chemical Rubber Co., Cleveland, 1967.
[18] E.M. Flanicen, H. Khatami, H.A. Szymanski, Adv. Chem. Ser. 101 (1971) 201.
[19] W.G. Ewing, Instrumental Methods of Chemical Analysis, fourth ed., McGraw-Hill, Kogakusha, 1975;
A.I. Vogel, A Text Book of Practical Organic Chemistry, third ed., Longman, 1975;
K. Nakamoto, Infrared Spectra of Inorganic and Coordination Compounds, second ed., Wiley-Interscience, 1970.
[20] L. Sacconi, M. Ciampolini, J. Chem. Soc. 276 (1964).
[21] (a) A.B.P. Lever, Inorganic Electronic Spectroscopy, Elsevier Publishing Company, Amsterdam, 1968;
(b) A.B.P. Lever, D. Ogden, J. Chem. Soc. 2041 (1967);
(c) L. Sacconi, I. Bertini, R. Morassi, Inorg. Chem. 6 (8) (1967) 1548.
[22] W.H. Quayle, J.H. Lunsford, Inorg. Chem. 21 (1982) 2226.
[23] W.H. Quayle, G. Peeters, G.L. De Roy, E.F. Vansant, J.H. Lunsford, Inorg. Chem. 21 (1982) 2226.
[24] M.N. Bae, M.K. Song, Y. Kim, Bull. Kor. Chem. Soc. 22 (2001) 1081.
[25] G.M. Schwab, E. Schwab-agallidis, J. Am. Chem. Soc. 17 (1949) 1806.
[26] S. Brunauer, L.S. Deming, W.S. Deming, E. Teller, J. Am. Chem. Soc. 62 (1940) 1723.
[27] (a) Z.M. El-Bahy, M.M. Mohamed, F.I. Zidan, M.S. Thabet, J. Hazard. Mater. 153 (2008) 364;
(b) M.M. Mokhtar, F.I. Zidan, M. Thabet, Micropor. Mesopor. Mater 108 (2008) 193.
[28] B. Neppolian, H.C. Choi, S. Sakthivel, V. Banumathi, A. Murugesan, J. Hazard. Mater. B89 (2002) 303.
[29] J.X. Chen, L.Z. Zhu, Catal. Today 126 (2007) 463.
[30] J.X. Chen, L.Z. Zhu, Chemosphere 65 (2006) 1249.
[31] C. Walling, A. Goosen, J. Am. Chem. Soc. 95 (1973) 2987.
[32] J. De Laat, H. Gallard, Environ. Sci. Technol. 33 (1999) 2726.